Noncoherent Integration for Signal Detection: Analysis Under Model Uncertainties

CHANDRASEKHAR JAYARAM

CHANDRA R. MURTHY, Senior Member, IEEE
Indian Institute of Science

The performance of postdetection integration (PDI) techniques for the detection of Global Navigation Satellite Systems (GNSS) signals in the presence of uncertainties in frequency offsets, noise variance, and unknown data-bits is studied. It is shown that the conventional PDI techniques are generally not robust to uncertainty in the data-bits and/or the noise variance. Two new modified PDI techniques are proposed, and they are shown to be robust to these uncertainties. The receiver operating characteristics (ROC) and sample complexity performance of the PDI techniques in the presence of model uncertainties are analytically derived. It is shown that the proposed methods significantly outperform existing methods, and hence they could become increasingly important as the GNSS receivers attempt to push the envelope on the minimum signal-to-noise ratio (SNR) for reliable detection.

Manuscript received March 26, 2012; revised September 4, 2012 and January 8, 2013; released for publication January 30, 2013.

IEEE Log No. T-AES/49/4/944708.

Refereeing of this contribution was handled by W. Blanding.

Authors' current addresses: C. Jayaram, Accord Software and Systems Pvt. Ltd., 37 K. R. Colony, Domlur Layout, Bangalore 560 071, India, E-mail: (chandrasekhar.j@accord-soft.com); C. R. Murthy, Department of Electrical and Computer Engineering, Indian Institute of Science, Bangalore 560 012, India.

I. INTRODUCTION

In a typical direct sequence code division multiple access (DS/CDMA) signal acquisition system, the synchronization between the incoming signal and the local pseudonoise sequence is achieved in two steps. In the first step, known as coarse synchronization or signal detection (which is the focus of this work), an initial estimate of code timing and frequency offset is obtained [1]. These coarse estimates are fine tuned to obtain the user position in the second stage of code tracking, typically using the time and frequency offset measurements [2]. During the coarse synchronization stage, the code delay and frequency uncertainty region is discretized into a finite number of cells, and the signal detection is carried out either sequentially or in parallel (or a combination of the two) [3, 4].

In general, the detection problem at an individual time-frequency block can be formulated as a composite hypothesis testing problem, where the signal-present hypothesis H_1 is parameterized by the timing and frequency offsets within the time-frequency block under test and the additive noise variance [5]. The noise-only hypothesis H_0 is parameterized by the noise variance. When the parameters are known, the likelihood ratio test (LRT) results in a coherent integration-based test statistic, also known as matched-filter detection. However, coherent integration for an arbitrarily long time duration is not possible in practice due to the presence of unknown data-bits and/or frequency uncertainty. The data-bits can be treated as known, for example, in assisted Global Navigation Satellite System (A-GNSS), wherein a reference receiver decodes the data-bits and sends them to the GNSS receiver over a communication network. However, in several practical scenarios, the receiver may have to operate in an unassisted mode [6, 7]. In this case it is difficult for the GNSS receiver itself to decode and collect the data-bits from all the visible satellites in challenging environments like high mobility scenarios, dense foliage, and urban canyons. Moreover, due to the sinusoidal modulation-type effect of frequency offset, the presence of frequency uncertainty also limits the coherent integration duration [1]. Other reasons for limiting the coherent integration duration include the presence of fading and user motion [8], and oscillator stability issues [9]. Hence, in this work, the coherent integration duration is restricted to be at most equal to the data-bit duration.

The output samples of the (partial) coherent integration stage are typically nonlinearly accumulated to enhance the sensitivity of detection under weak signal conditions, leading to a class of methods known as postdetection integration (PDI) or postcoherent integration techniques [10]. The two most widely

used PDI techniques are the noncoherent PDI (NC-PDI) [11] and the differential PDI (D-PDI) technique [12]. Although these techniques are now well known, a detailed analysis of their performance in the presence of timing, frequency, noise, data-bit, and other model uncertainties has not been fully characterized. In addition, it is of practical importance to devise algorithms for signal detection that are robust to the commonly encountered uncertainties and that can work reliably at low signal-to-noise ratios (SNRs) (for example, in GNSS signal acquisition). Thus, the goals of this work are twofold: to rigorously analyze the performance of the existing PDI techniques for weak signal detection in the presence of model uncertainties and to develop novel PDI techniques that are robust to model uncertainties. The model uncertainties considered in this work are timing, frequency, noise, and data-bit uncertainties, with the primary emphasis on the latter two uncertainties.

The problem of noise variance and SNR estimation has been studied by several authors (e.g., [15]–[17]). In DS/CDMA systems, uncertainty in the noise variance naturally arises as they are often used in multi-application systems, and the aggregate interference from a host of other systems causes variations in the noise level. It could also arise due to unintentional jamming from wireless local area network (WLAN) or long-term evolution (LTE) transceivers that may be implemented on the same chip or due to interference from other higher power satellite signals since the pseudorandom chip sequences are not perfectly orthogonal. Noise variance uncertainty can lead to fundamental limits on the minimum SNR for reliable signal detection [13, 14].

Since reliable detection of unknown data-bits is not possible at low SNR, the maximum coherent integration duration is typically limited to the data bit period. In [18], a cyclostationarity-based test statistic was proposed and was shown to be robust in the presence of data-bits. In this work, we therefore primarily focus on the effect of noise and data-bit uncertainties on the performance of PDI-based signal detection.

The effect of timing and frequency uncertainty on signal detection has been studied in the past (see, e.g., [1], [19], [20]). Extending the duration of coherent integration under frequency uncertainty leads to degradation in the signal energy, which can be mitigated by searching over a larger number of frequency bins to improve the frequency resolution, at the cost of a longer total dwell time for a given detection performance [21]. Timing uncertainty arises because a finite subset of possible fractional code chip spacings are searched in a parallel/sequential manner [22]. While the timing uncertainty also leads to a loss of signal energy, it does not impose a fundamental limit on signal detection.

In the context of the above, the main contributions of this paper are as follows:

1) For quadratic and nonquadratic forms of the NC-PDI technique, by analyzing the false alarm and detection performance, it is shown in Section III that noise uncertainty leads to a lower limit on the SNR for reliable detection. The NC-PDI techniques are inherently insensitive to the presence of unknown data-bits due to the magnitude computation in the test statistic.

2) In contrast the D-PDI technique is shown to be robust to noise uncertainty in Section IV. However, when uncertainty in the data-bits is considered, it is shown that unlike the NC-PDI, the D-PDI is not a robust detection technique.

3) In Section V, a different and better performing modified PDI technique is proposed, where the coherent integration duration can extend up to the data-bit duration. Two forms of the modified PDI are proposed, for data and pilot channels.

4) The false alarm and miss detection probability performance of the three conventional and the two proposed detectors are analyzed in the presence of model uncertainties.

5) Approximate expressions for the sample complexity, which has a direct effect on the detection delay, are derived in the presence of noise uncertainty, using Gaussian approximations.

Although the analysis presented here is applicable to any DS/CDMA system, in this paper, we focus our discussion on GNSS signal detection as an example application. We validate our theoretical results through Monte Carlo simulations and present the results in Section VI. In particular, we illustrate that for current GNSS signal acquisition systems, the state-of-the-art performance is within 3 dB of the SNR limit imposed by noise uncertainty due to a 0.3 dB uncertainty in the interference level. Our proposed modified PDI techniques, which are insensitive to uncertainty in the noise variance and data-bits, are therefore likely to become important as the system designers attempt to push the envelope on the minimum SNR for reliable detection. We offer some concluding remarks in Section VII.

II. SIGNAL MODEL

The received signal sampled at nT_s can be represented in the complex baseband form as [5]

$$r[n] = \sum_{k=1}^{K} \sqrt{P_k} c_k[nT_s - \tau_k] b_k[nT_s - \tau_k] \times \exp(j(2\pi f_{d_k} nT_s + \theta_k)) + w[n] \quad (1)$$

where P_k is the received signal power, $c_k[nT_s - \tau_k]$ is the pseudorandom code sequence, $b_k[nT_s - \tau_k]$ is the unknown data-bit that spans multiple T_s durations, τ_k is the code delay, f_{d_k} is the frequency offset due to both the clock mismatch between the transmitter and the receiver as well as the Doppler effect, θ_k is the carrier phase of the signal received from the kth transmitter (kth satellite in GNSS), K is the number of transmitters, and $w[n]$ is the noise sequence, modeled as samples from an independent and identically distributed (i.i.d.) white Gaussian noise process. In the coherent integration stage, the frequency offset is partially compensated for using the complex exponential $\exp(-j2\pi\hat{f}_{d_k} nT_s)$, and the resulting signal is correlated with a replica of the pseudorandom sequence of the kth transmitter $c_k(nT_s - \hat{\tau}_k)$, where $\hat{f}_{d_k}$ and $\hat{\tau}_k$ are hypotheses on the frequency and code timing offset, respectively. These signal samples are coherently integrated for N_{coh} samples to get [23]

$$x[m] = N_{\text{coh}}\sqrt{P}\,\text{sinc}(\Delta f T_{\text{coh}})b[m] \times \exp(j(2\pi m \Delta f T_{\text{coh}} + \theta))R(\Delta\tau) + w_{\text{coh}}[m] \tag{2}$$

where $x[m]$ is the output of the coherent integration stage at time $mN_{\text{coh}}T_s$, $N_{\text{coh}} \triangleq f_s T_{\text{coh}}$ is the sample complexity of the coherent integration stage, $f_s \triangleq 1/T_s$ is the sampling frequency, and T_{coh} is the coherent integration duration. Also, the effective noise $w_{\text{coh}}[m]$ includes the components from both the so-called self-noise (see [12]) and the additive white Gaussian noise (AWGN). In (2), the index k of the code sequence of interest (for example, the kth satellite in GNSS signal detection) has been dropped for simplicity, and $\Delta f \triangleq f_{\text{d}} - \hat{f}_{\text{d}}$ is the residual frequency offset. The $\text{sinc}(\Delta f T_{\text{coh}})$ term captures the degradation in signal energy due to the residual frequency offset [10]. Also, $R(\Delta\tau) \triangleq (1 - |\Delta\tau|/T_c)$, for $|\Delta\tau| \le T_c$ and 0 otherwise, is the triangular auto-correlation function with pseudorandom code offset $\Delta\tau = \tau - \hat{\tau}$, and T_c is the code chip duration. The unknown data-bit $b[m] \in \{+1, -1\}$, and as mentioned earlier, $b[m]$ spans a duration T_b which is typically an integer multiple of T_{coh}. Further, in the sequel, it is assumed that the bit transition boundaries are known (for example, from a previous successful acquisition by the receiver, which is typical in GNSS signal detection), due to which, there is no bit transition within the coherent integration duration. The uncertainty in the data bit transition boundary would result in a corresponding reduction in the coherent integration duration. Acquisition of the bit transition boundaries in an unassisted GPS scenario is discussed in [24], [25].

Now, due to the pseudorandom nature of the chip sequence and the Gaussian nature of the noise, the signal $x[m]$ is modeled as a complex Gaussian distributed sequence of independent random variables under both the hypotheses

$$x[m] \sim \begin{cases} \mathcal{CN}(0, N_{\text{coh}}\sigma^2) & \text{under } H_0 \\ \mathcal{CN}(\mu_x[m]e^{j\theta}, N_{\text{coh}}\sigma^2) & \text{under } H_1 \end{cases} \tag{3}$$

where $\mathcal{CN}(m, s^2)$ represents the complex Gaussian distribution with mean m and variance s^2, $\mu_x[m] = N_{\text{coh}}\sqrt{P}\,\text{sinc}(\Delta f T_{\text{coh}})b[m]e^{j2\pi m \Delta f T_{\text{coh}}}R(\Delta\tau)$, and σ^2 is the effective noise variance at the input of the coherent integration stage.

A. Noise Uncertainty

In a practical receiver, the noise variance σ^2 is typically estimated using the observations under H_0, the noise-only hypothesis. The estimated noise variance may not be exact due to the limited number of samples used in the estimation process, changes in the ambient temperature and/or interference level, unintentional jamming from other systems such as WLAN, LTE, etc. This uncertainty in the noise variance can make the detector nonrobust and can impose a fundamental limitation on the minimum SNR for reliable signal detection (referred to as the SNR wall), which cannot be alleviated by increasing the sample complexity [13, 14]. The noise uncertainty model that is typically used is as follows. The nominal noise probability density function (pdf) is represented as $w[n] \sim \mathcal{CN}(0, \sigma_n^2)$, and the actual noise variance is assumed to lie in $[(1/\beta)\sigma_n^2, \beta\sigma_n^2]$, where $\beta > 1$ is a parameter that quantifies the amount of uncertainty present in the noise. In general reliable detection is not possible if and only if [13]

$$\min_{\sigma^2 \in [(1/\beta)\sigma_n^2, \beta\sigma_n^2]} E\{T \mid H_1\} \le \max_{\sigma^2 \in [(1/\beta)\sigma_n^2, \beta\sigma_n^2]} E\{T \mid H_0\} \tag{4}$$

for all M, where $E\{\cdot\}$ is the expectation operator and T is the test statistic computed from M coherent integration output samples. The noise floor fluctuations modeled as in [13] are used to analyze the different PDI techniques used in GNSS signal detection. The analysis of the performance of the NC-PDI technique in this paper is similar to that in [13], as the focus of the latter was on energy detection. However, the analysis of the robustness of the other PDI techniques to noise variance and data-bit uncertainties, as well as the proposed new

detectors that are robust to these uncertainties, are novel in this work.

III. NONCOHERENT PDI

NC-PDI is similar to energy detection and is the most widely used PDI technique. In this section it is shown that a fundamental sensitivity limit exists in the two forms of the NC-PDI technique, namely, the quadratic NC-PDI and the nonquadratic NC-PDI, in the presence of noise uncertainty.

A. Quadratic NC-PDI

In this subsection, we first present the false alarm and detection probability performance of the NC-PDI, and then show that noise uncertainty results in a fundamental SNR wall on reliable detection. We also obtain an approximate expression for the sample complexity M required to attain a given P_{fa} and P_{d}. The test statistic is the square of the envelope of the coherent integration output samples, i.e.,

$$T_{B1} \triangleq \sum_{k=1}^{M} |x[k]|^2 \tag{5}$$

where $x[k]$ is as defined in (2). Under the statistical model in (3), the distribution of T_{B1} is central χ^2 with $2M$ degrees of freedom under H_0 and noncentral χ^2 with $2M$ degrees of freedom under H_1. The expressions for the false alarm and detection probabilities are [11]

$$\begin{aligned} P_{\text{fa}} &= \exp\left(-\frac{\gamma}{2N_{\text{coh}}\sigma^2}\right)\sum_{k=0}^{M-1}\frac{1}{k!}\left(\frac{\gamma}{2N_{\text{coh}}\sigma^2}\right)^k \\ P_{\text{d}} &= Q_M\left(\sqrt{\frac{\lambda}{N_{\text{coh}}\sigma^2}}, \sqrt{\frac{\gamma}{N_{\text{coh}}\sigma^2}}\right) \end{aligned} \tag{6}$$

where γ is the detection threshold on T_{B1}, $\lambda = MN_{\text{coh}}^2 PD(\Delta f, \Delta\tau)$ is the noncentrality parameter that also represents the signal energy in the coherent integration output samples, and $Q_M(a,b)$ is the generalized Marcum-Q function [26]. Here, the term $D(\Delta f, \Delta\tau) \leq 1$ captures the loss in signal power due to timing and frequency uncertainty and is given by $D(\Delta f, \Delta\tau) \triangleq [\text{sinc}(\Delta f T_{\text{coh}})R(\Delta\tau)]^2$, with $R(\Delta\tau)$ as defined in the previous section [1]. The accuracy of the P_{fa} and P_{d} expressions above is illustrated through Monte Carlo simulations in Section VI.

Now, to analyze the effect of noise uncertainty on the NC-PDI technique, the mean and variance of T_{B1} given by (5) under the null and alternate hypothesis can be expressed as

$$\begin{aligned} E\{T_{B1} \mid H_0\} &= 2M(N_{\text{coh}}\sigma^2) \\ \text{Var}\{T_{B1} \mid H_0\} &= 4M(N_{\text{coh}}\sigma^2)^2 \\ E\{T_{B1} \mid H_1\} &= MN_{\text{coh}}^2 PD(\Delta f, \Delta\tau) + 2MN_{\text{coh}}\sigma^2 \\ \text{Var}\{T_{B1} \mid H_1\} &= 4M((N_{\text{coh}}^2 P)D(\Delta f, \Delta\tau)(N_{\text{coh}}\sigma^2) + (N_{\text{coh}}\sigma^2)^2). \end{aligned} \tag{7}$$

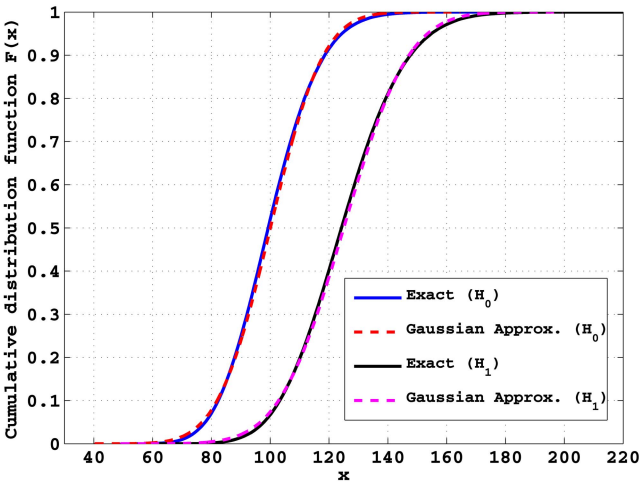

Fig. 1. Empirical cdf to validate Gaussian approximation to cdf of NC-PDI (quadratic), $M = 50$, $\rho_{\text{coh}} = -3$ dB.

Using (4), it is easy to show that the SNR wall is given by

$$\text{SNR}_L = \frac{2}{N_{\text{coh}}D(\Delta f, \Delta\tau)}\left(\beta - \frac{1}{\beta}\right) \tag{8}$$

where $\text{SNR}_L \triangleq P/\sigma_n^2$ is the SNR of the samples at the input of the coherent integration stage and σ_n^2 is the nominal noise variance. As mentioned earlier, increasing N_{coh} is not an option for decreasing SNR_L due to the presence of unknown data-bits and/or frequency uncertainty. The coherent integration duration can at most be the data-bit period since the navigation data-bits are a priori unknown, and their estimation is not possible at low SNR conditions. Also, due to the sinusoidal modulation-type effect of the frequency offset, the presence of residual frequency uncertainty also limits N_{coh}.

Another parameter of interest is the sample complexity M to achieve a desired P_{fa} and P_{d} in the presence of noise uncertainty, as the sample complexity has a direct impact on the time-to-detect of the receiver. However, the expressions of P_{d} and P_{fa} in (6) are analytically intractable for directly deriving the sample complexity. Hence, we use the fact that $|x[k]|^2$ are i.i.d. with finite variance and apply the central limit theorem (CLT) (as in [27]) to get approximations for P_{fa} and P_{d} as

$$\begin{aligned} P_{\text{fa}}(\sigma^2) &\approx Q\left(\frac{\gamma - 2MN_{\text{coh}}\sigma^2}{\sqrt{4M}(N_{\text{coh}}\sigma^2)}\right) \\ P_{\text{d}}(\sigma^2) &\approx Q\left(\frac{\gamma - M(N_{\text{coh}}^2 P + 2(N_{\text{coh}}\sigma^2))}{\sqrt{4M((N_{\text{coh}}\sigma^2)^2 + N_{\text{coh}}^3 P\sigma^2)}}\right) \end{aligned} \tag{9}$$

where $Q(x) = (1/\sqrt{2\pi})\int_x^\infty \exp\{-y^2/2\}dy$ is the Gaussian Q-function. To simplify the analysis of the sample complexity in the presence of noise uncertainty, the effect of frequency and timing uncertainty is neglected. The accuracy of the Gaussian approximation is illustrated in Fig. 1 by plotting

empirical and the approximate Gaussian cumulative distribution functions (cdfs) for $M = 50$ and at an SNR at the output of the coherent integration stage of -3 dB. The value of $M \geq 50$ is typical in GNSS applications for detection of weak signals [28–30]. Now, under the noise uncertainty model, it is required that the target P_{fa} and P_{d} be satisfied over the entire range of noise uncertainty values. In this case, the number of noncoherent accumulations required to achieve the desired P_{fa} and P_{d} can be evaluated as

$$\begin{aligned} P_{\text{fa},nu} &\triangleq \max_{\sigma^2 \in [(1/\beta)\sigma_n^2, \beta\sigma_n^2]} P_{\text{fa}}(\sigma^2) = Q\left(\frac{\gamma - 2M(N_{\text{coh}}\beta\sigma_n^2)}{\sqrt{4M}(N_{\text{coh}}\beta\sigma_n^2)}\right) \\ P_{d,nu} &\triangleq \min_{\sigma^2 \in [(1/\beta)\sigma_n^2, \beta\sigma_n^2]} P_{\text{d}}(\sigma^2) \\ &= Q\left(\frac{\gamma - M\left(N_{\text{coh}}^2 P + 2\left(N_{\text{coh}}\frac{1}{\beta}\sigma_n^2\right)\right)}{\sqrt{4M\left(\left(N_{\text{coh}}\frac{1}{\beta}\sigma_n^2\right)^2 + \left(N_{\text{coh}}^3 P\frac{1}{\beta}\sigma_n^2\right)\right)}}\right). \end{aligned} \tag{10}$$

Solving for γ to achieve the required $P_{\text{fa},nu}$, substituting it in the expression for $P_{d,nu}$, and solving for the sample complexity of noncoherent accumulations, we get

$$M = \frac{4\left(Q^{-1}(P_{\text{fa},nu})\beta - Q^{-1}(P_{d,nu})\sqrt{\frac{1}{\beta}\rho_{\text{coh}} + \frac{1}{\beta^2}}\right)^2}{\left(\rho_{\text{coh}} - 2\left(\beta - \frac{1}{\beta}\right)\right)^2} \tag{11}$$

where $\rho_{\text{coh}} \triangleq N_{\text{coh}}P/\sigma_n^2$ is the SNR at the coherent integration output. From the above expression it is clear that as $\rho_{\text{coh}} \to 2(\beta - 1/\beta)$, $M \to \infty$. Thus, the NC-PDI has an SNR limit due to noise uncertainty.

B. Nonquadratic NC-PDI

In this subsection, the performance of a nonquadratic form of the NC-PDI is analyzed in the presence of noise uncertainty. We first analyze the first- and second-order moments of the test statistic to show that noise uncertainty imposes a fundamental SNR wall on reliable detection. Then, we obtain an expression for the sample complexity required to attain a given P_{fa} and P_{d} using Gaussian approximations. The test statistic is given by

$$T_{B2} \triangleq \sum_{k=1}^{M} |x[k]|. \tag{12}$$

The main advantage of T_{B2} is its ease of implementation, as good approximations exist for computing the envelope $|x[k]|$. From (3), $|x[k]|$ is Rayleigh distributed under H_0 and Ricean distributed under H_1. The mean and variance of T_{B2} under both the hypotheses are expressed as [31]

$$\begin{aligned} E\{T_{B2} \mid H_0\} &= M\sqrt{\frac{\pi N_{\text{coh}}\sigma^2}{2}} \\ \text{Var}\{T_{B2} \mid H_0\} &= M\left(\frac{4-\pi}{2}\right)N_{\text{coh}}\sigma^2 \end{aligned} \tag{13}$$

$$\begin{aligned} E\{T_{B2} \mid H_1\} &= M\sqrt{\frac{\pi N_{\text{coh}}\sigma^2}{2}} \\ &\quad \times e^{-\rho_s/4}\left[\left(1 + \frac{\rho_s}{2}\right)I_0\left(\frac{\rho_s}{4}\right) + \frac{\rho_s}{2}I_1\left(\frac{\rho_s}{4}\right)\right] \end{aligned} \tag{14}$$

$$\text{Var}\{T_{B2} \mid H_1\} = M\left(2N_{\text{coh}}\sigma^2\left(1 + \frac{\rho_s}{2}\right) - (E\{T_{B2} \mid H_1\})^2\right) \tag{15}$$

where $\rho_s \triangleq N_{\text{coh}}P/\sigma^2$. From (4), an SNR limit exists if and only if

$$\begin{aligned} &\sqrt{\frac{\pi N_{\text{coh}}\frac{1}{\beta}\sigma_n^2}{2}}e^{-\beta\rho_{\text{coh}}/4}\left[\left(1 + \frac{\beta\rho_{\text{coh}}}{2}\right)I_0\left(\frac{\beta\rho_{\text{coh}}}{4}\right)\right. \\ &\qquad \left. + \frac{\beta\rho_{\text{coh}}}{2}I_1\left(\frac{\beta\rho_{\text{coh}}}{4}\right)\right] \\ &\quad \leq \sqrt{\frac{\pi N_{\text{coh}}\beta\sigma_n^2}{2}} \end{aligned} \tag{16}$$

where $\rho_{\text{coh}} \triangleq N_{\text{coh}}P/\sigma_n^2$, as before. Subtracting $\sqrt{\pi N_{\text{coh}}(1/\beta)\sigma_n^2/2}$ on both the sides above,

$$\begin{aligned} &\frac{1}{\sqrt{\beta}}\left(e^{-\beta\rho_{\text{coh}}/4}\left[\left(1 + \frac{\beta\rho_{\text{coh}}}{2}\right)I_0\left(\frac{\beta\rho_{\text{coh}}}{4}\right)\right.\right. \\ &\qquad \left.\left. + \frac{\beta\rho_{\text{coh}}}{2}I_1\left(\frac{\beta\rho_{\text{coh}}}{4}\right)\right] - 1\right) \\ &\quad \leq \left(\sqrt{\beta} - \frac{1}{\sqrt{\beta}}\right). \end{aligned} \tag{17}$$

The above expression involves the Bessel functions of the zeroth and first orders and is analytically intractable. To evaluate the SNR wall, we resort to a polynomial approximation at low SNR [31] to get

$$\frac{1}{\sqrt{\beta}}\left(\frac{\beta\rho_{\text{coh}}}{4} - \frac{(\beta\rho_{\text{coh}})^2}{96} + \frac{(\beta\rho_{\text{coh}})^3}{768}\right) \leq \left(\sqrt{\beta} - \frac{1}{\sqrt{\beta}}\right). \tag{18}$$

For detection of weak signals, the postcoherent SNR $\rho_{\text{coh}} \ll 1$. Neglecting higher order terms in the above expression, if $\rho_{\text{coh}} \leq 4(1 - 1/\beta)$, the sample complexity of nonquadratic NC-PDI becomes unbounded. However, the approximation does not hold for higher values of $\beta\rho_{\text{coh}}$, and this is illustrated in Fig. 2. In the figure, the curve marked Approx. (1)—Theory refers to the SNR wall obtained by numerically solving for the equality condition in (18), and the curve marked Approx. (2)—Theory refers to $\rho_{\text{coh}} = 4(1 - 1/\beta)$. However, finding a

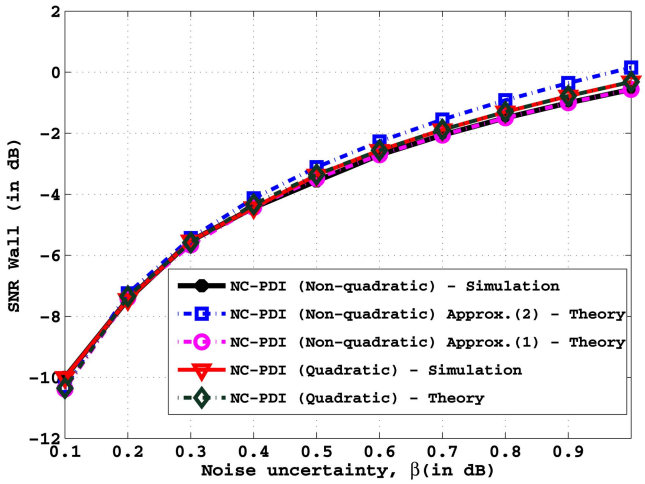

Fig. 2. SNR wall: exact expression versus approximation for nonquadratic NC-PDI technique, and comparison of theoretical and simulation-based values for quadratic NC-PDI.

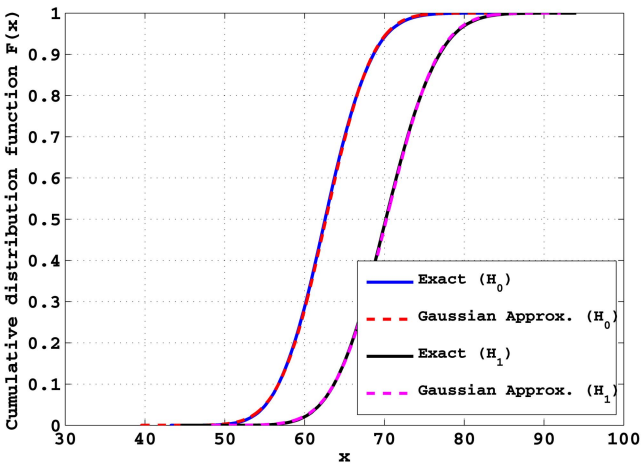

Fig. 3. Empirical cdf to validate Gaussian approximation to cdf of NC-PDI (nonquadratic), $M = 50$, $\rho_{\text{coh}} = -3$ dB.

closed-form expression for the sample complexity required to achieve a desired performance is difficult as no closed-form solution exists for the distribution of the sum of i.i.d. Rayleigh and Ricean random variables. Hence, we follow a similar procedure as the previous subsection and employ Gaussian approximations on the cdf of the test statistic since the terms in the summation $|x[k]|$ are i.i.d. and have finite variance. The accuracy of the Gaussian cdf is illustrated in Fig. 3, for $M = 50$ and a coherent SNR of -3 dB, and it can be seen that the error in the approximation is negligible. Hence, the expressions for P_{fa} and P_{d} in the presence of noise uncertainty can be obtained as in the previous subsection as

$$P_{\text{fa},nu} \approx Q\left(\frac{\gamma - M\sqrt{\frac{\pi N_{\text{coh}}\beta\sigma_n^2}{2}}}{\sqrt{M\left(\frac{4-\pi}{2}\right)N_{\text{coh}}\beta\sigma_n^2}}\right) \tag{19}$$

$$P_{d,nu} \approx Q\left(\frac{\gamma - M\sqrt{\frac{\pi N_{\text{coh}}}{2}\frac{1}{\beta}\sigma_n^2}\,e^{(-\beta\rho_{\text{coh}}/4)}\left[\left(1+\frac{\beta\rho_{\text{coh}}}{2}\right)I_0\left(\frac{\beta\rho_{\text{coh}}}{4}\right)+\frac{\beta\rho_{\text{coh}}}{2}I_1\left(\frac{\beta\rho_{\text{coh}}}{4}\right)\right]}{\sqrt{M\left(N_{\text{coh}}\sigma_n^2\left(\rho_{\text{coh}}+\frac{2}{\beta}\right)-\left(E\left\{\left(T_{B2},\frac{1}{\beta}\right)\mid H_1\right\}\right)^2\right)}}\right) \tag{20}$$

where $E\{(T_{B2}, 1/\beta) \mid H_1\}$ is the mean of the test statistic T_{B2}, given by (14), but with σ_n^2/β instead of σ^2 as the noise variance. From the above expressions, sample complexity M is given by

$$M \approx \frac{\left(Q^{-1}(P_{\text{fa},nu})\sqrt{\left(\frac{4-\pi}{2}\right)\beta} - Q^{-1}(P_{d,nu})\sqrt{\left(\left(\rho_{\text{coh}}+\frac{2}{\beta}\right)-\frac{1}{N_{\text{coh}}\sigma_n^2}\left(E\left\{\left(T_{B2},\frac{1}{\beta}\right)\mid H_1\right\}\right)^2\right)}\right)^2}{\frac{\pi}{2}\left(\frac{1}{\sqrt{\beta}}e^{(-\beta\rho_{\text{coh}}/4)}\left[\left(1+\frac{\beta\rho_{\text{coh}}}{2}\right)I_0\left(\frac{\beta\rho_{\text{coh}}}{4}\right)+\frac{\beta\rho_{\text{coh}}}{2}I_1\left(\frac{\beta\rho_{\text{coh}}}{4}\right)\right]-\sqrt{\beta}\right)^2}. \tag{21}$$

It is illustrated in Section VI that the sample complexity expression derived above closely matches the simulation-based results.

IV. DIFFERENTIAL PDI

In this section, the performance of the D-PDI technique is analyzed in the presence of noise uncertainty. The real part of the 1-span D-PDI (defined below) is known to be robust to frequency offsets of relatively small magnitude, i.e., $\Delta f T_{\text{coh}} <$

0.125. For larger frequency offsets the absolute value of the 1-span D-PDI is used as test statistic [20]. This is extended to using the sum of D-PDI terms with multiple spans as test statistic [32]. However, here we consider the real part of the 1-span D-PDI as the test statistic [20]:

$$T_C \triangleq \mathrm{Re}\left\{\sum_{k=2}^{M} x[k]x^*[k-1]\right\}. \tag{22}$$

In the above, $x[k]$ represents the output of coherent integration for half the data-bit duration. The performance of the 1-span D-PDI was analyzed in [19], and it was found that in the presence of time and small frequency offsets, the performance is similar to that of the NC-PDI. Hence, we analyze its performance in the presence of noise uncertainty in the sequel.

A. Analytical Characterization

Here, we derive a closed-form expression for P_{fa} for the 1-span D-PDI. We also present a method to evaluate the P_{d} numerically, using the characteristic function. The D-PDI test statistic T_C can be expressed as a linear combination of independent χ^2 random variables $y[k]$ (see Appendix, Subsection A),

$$T_C = \sum_{k=1}^{M} \lambda_k |y[k]|^2 \tag{23}$$

where $y[k] = v_k^H X$, v_k (given by (56) in the Appendix) is the eigenvector of a tridiagonal matrix corresponding to its eigenvalue λ_k and $X \triangleq [x[1], x[2], \ldots, x[M]]^T$. Under H_0, it can be shown that $y[k]$ are i.i.d. Gaussian distributed, and hence the characteristic function of T_C is given by [33]

$$\begin{aligned}\phi_{T_C,H_0}(\omega) &= \prod_{k=1}^{M} \frac{1}{(1 - j2\lambda_k N_{\mathrm{coh}}\sigma^2\omega)} \\ &= \sum_{k=1}^{M} \frac{C_k}{1 - j2\lambda_k N_{\mathrm{coh}}\sigma^2\omega}\end{aligned} \tag{24}$$

where

$$C_k = \prod_{m=1, m\neq k}^{M} \frac{\cos\left(\frac{\pi k}{M+1}\right)}{\cos\left(\frac{\pi k}{M+1}\right) - \cos\left(\frac{\pi m}{M+1}\right)}.$$

The pdf is obtained by evaluating the inverse Fourier transform at $-y$. Subsequently, P_{fa} can be derived as follows

$$\begin{aligned}P_{\mathrm{fa}} = \int_{\gamma}^{\infty} \sum_{k=1}^{M} \frac{1}{2\pi} \int_{-\infty}^{\infty} \frac{C_k}{(1 - j2\lambda_k N_{\mathrm{coh}}\sigma^2\omega)} \\ \times \exp(-j\omega y) d\omega\, dy\end{aligned} \tag{25}$$

where γ is the detection threshold. Since there are both negative and positive eigenvalues, the P_{fa} expression is modified as

$$P_{\mathrm{fa}} = \int_{\gamma}^{\infty} \sum_{k=1}^{M} \frac{C_k}{2\lambda_k N_{\mathrm{coh}}\sigma^2} \exp\left(\frac{-\mathrm{sgn}(\lambda_k)y}{2\lambda_k N_{\mathrm{coh}}\sigma^2}\right) u(\mathrm{sgn}(\lambda_k)y) dy \tag{26}$$

where $\mathrm{sgn}(x) \triangleq 1$ if $x \geq 0$ and -1 otherwise; and $u(y) \triangleq 1$ if $y \geq 0$ and 0 otherwise. Evaluating the integral we get the expression for the probability of false alarm for the 1-span D-PDI as

$$P_{\mathrm{fa}} = \begin{cases} \displaystyle\sum_{k=1,\lambda_k>0}^{M} C_k \exp\left(-\frac{\gamma}{2\lambda_k N_{\mathrm{coh}}\sigma^2}\right), & \gamma > 0 \\ \displaystyle 1 - \sum_{k=1,\lambda_k<0}^{M} C_k \left(\exp\left(-\frac{\gamma}{2\lambda_k N_{\mathrm{coh}}\sigma^2}\right)\right), & \gamma < 0. \end{cases} \tag{27}$$

Thus, the probability of false alarm of the 1-span D-PDI can be evaluated. To evaluate the probability of detection, under H_1, a closed-form expression cannot be found for the distribution of the weighted linear combination of noncentral χ^2 random variables except when $M = 2$. Note that T_C can be expressed in an alternate form (see Appendix, Subsection A) as

$$T_C = \sum_{k=1}^{\tilde{M}} \lambda_k (|y_p[k]|^2 - |y_n[k]|^2) \tag{28}$$

where $\tilde{M} \triangleq M/2$, $y_p[k] \triangleq y[k]1_{\lambda_k>0}$, $y_n[k] \triangleq y[k]1_{\lambda_k<0}$, and 1_A is an indicator function, taking the value 1 when A is true and 0 otherwise. When $M = 2$ (or $\tilde{M} = 1$), it is easy to show that $|y_n[1]|^2 = (x[2] - x[1])^2/4$ is central χ^2 distributed and $|y_p[1]|^2 = (x[2] + x[1])^2/4$ is noncentral χ^2 distributed [26]. From this, an expression for P_{d} can be obtained.

For $\tilde{M} > 1$, the characteristic function of T_C has to be numerically inverted, as explained below. The characteristic function is given by [34]

$$\begin{aligned}\phi_{T_C,H_1}(\omega) = \exp\left(-\frac{1}{2}\sum_{k=1}^{M}\mu_{y_k}^2 + \frac{1}{2}\sum_{k=1}^{M}\frac{\mu_{y_k}^2}{1 - j2\lambda_k N_{\mathrm{coh}}\sigma^2\omega}\right) \\ \times \prod_{k=1}^{M} \frac{1}{(1 - j2\lambda_k N_{\mathrm{coh}}\sigma^2\omega)}\end{aligned} \tag{29}$$

where $\mu_{y_k}^2$ is the noncentrality parameter of $|y[k]|^2$, which is computed from the data signal. The expression for P_{d} can now be obtained numerically as

$$P_{\mathrm{d}} = \frac{1}{2} + \frac{1}{\pi}\int_0^{\infty} \frac{\sin(\theta(u))}{uc(u)} du \tag{30}$$

where $\theta(u)$ and $c(u)$ are derived from the characteristic function in (29) as

$$\theta(u) = \sum_{k=1}^{M} \left[\tan^{-1}(2\lambda_k N_{\text{coh}} \sigma^2 u) + \frac{\mu_{y_k}^2 \lambda_k N_{\text{coh}} \sigma^2 u}{(1 + 4\lambda_k^2 N_{\text{coh}}^2 \sigma^4 u^2)} \right] - \gamma u$$

$$c(u) = \prod_{k=1}^{M} [(1 + 4\lambda_k^2 N_{\text{coh}}^2 \sigma^4 u^2)^{1/2}] \times \exp\left(\frac{1}{2} \sum_{k=1}^{M} \frac{(\mu_{y_k} 2\lambda_k N_{\text{coh}} \sigma^2 u)^2}{(1 + 4\lambda_k^2 N_{\text{coh}}^2 \sigma^4 u^2)} \right). \tag{31}$$

The computation of the sample complexity from the above expressions is possible through numerical methods. To gain further insight into the sample complexity, a Gaussian approximation is used, which is described in the next subsection.

REMARK The above analytical characterization can, in principle, be extended to n-span D-PDI ($n > 1$), and for the linear combination of D-PDIs computed at multiple spans. However, a closed form expression for the eigenvalues of the resulting banded Toeplitz matrix is not available [35].

B. Sample Complexity of the 1-Span D-PDI

In this subsection, we first characterize the second-order statistics of the test statistic T_C given by (22) and then use the CLT arguments as before to obtain approximate expressions for the sample complexity. The test statistic T_C can be expressed as a combination of two test statistics by separating the even and odd terms, i.e., $T_C = T_{C1} + T_{C2}$, where

$$T_{C1} \triangleq \text{Re}\left\{ \sum_{k=1}^{M/2} x[2k] x^*[2k-1] \right\}$$
$$T_{C2} \triangleq \text{Re}\left\{ \sum_{k=1}^{(M/2)-1} x[2k+1] x^*[2k] \right\}. \tag{32}$$

In the analysis that follows, it is assumed that M is even (the analysis easily extends to the case where M is odd). Let $x[k] = x_I[k] + j x_Q[k]$, with $x_I[k]$ and $x_Q[k]$ being the in-phase (real) and quadrature (imaginary) components of the coherent integration output at time k, respectively. The test statistics T_{C1} and T_{C2} can be rewritten as

$$T_{C1} = \sum_{k=1}^{M/2} x_I[2k] x_I[2k-1] + x_Q[2k] x_Q[2k-1]$$
$$T_{C2} = \sum_{k=1}^{(M/2)-1} x_I[2k+1] x_I[2k] + x_Q[2k+1] x_Q[2k]. \tag{33}$$

It was shown by the authors in [14] that

$$\begin{aligned} E\{T_{C1} \mid H_0\} &= 0 \\ \text{Var}\{T_{C1} \mid H_0\} &= M N_{\text{coh}}^2 \sigma^4 \\ E\{T_{C1} \mid H_1\} &= \frac{M}{2} N_{\text{coh}}^2 P \\ \text{Var}\{T_{C1} \mid H_1\} &= M N_{\text{coh}}^2 \sigma^4 + M N_{\text{coh}}^3 P \sigma^2. \end{aligned} \tag{34}$$

The mean and the variance of T_{C2} is similar to T_{C1} except that M is replaced by $M-2$. Now, to complete the second-order statistical description of T_C, we need the cross-covariance between T_{C1} and T_{C2} (denoted as $\text{Cov}\{T_{C1}, T_{C2}\}$), under either hypothesis. The cross-covariance can be found by evaluating $E\{T_{C1} T_{C2}\}$, and the details are shown in the Appendix, Subsection B. Using this, it can be shown that the mean and variance of the 1-span D-PDI test statistic T_C under both the hypotheses are given by

$$\begin{aligned} E\{T_C \mid H_0\} &= 0 \\ \text{Var}\{T_C \mid H_0\} &= 2(M-1) N_{\text{coh}}^2 \sigma^4 \\ E\{T_C \mid H_1\} &= (M-1) N_{\text{coh}}^2 P \\ \text{Var}\{T_C \mid H_1\} &= 2(M-1) N_{\text{coh}}^2 \sigma^4 + 2(2M-3) N_{\text{coh}}^3 P \sigma^2. \end{aligned} \tag{35}$$

As in Section III, we approximate the distribution of T_C by a Gaussian distribution under both hypotheses. Note that the terms within T_{C1} are i.i.d. with finite variance, and the same holds for the terms in T_{C2}, but T_{C1} is not independent of T_{C2}. By the CLT, T_{C1} and T_{C2} can be approximated as Gaussian distributed, and hence their sum can also be approximated as Gaussian distributed. Figure 4 compares the Gaussian approximation with the empirical cdf, and it can be seen that at $M = 50$ and a coherent SNR of -3 dB, the approximation error is negligible. Hence, the sample complexity M in the presence of noise uncertainty can be approximated as

$$M \approx 1 + \frac{2\left(Q^{-1}(P_{\text{fa},nu})\beta - Q^{-1}(P_{d,nu}) \sqrt{\frac{2\rho_{\text{coh}}}{\beta} + \frac{1}{\beta^2}} \right)^2}{\rho_{\text{coh}}^2}. \tag{36}$$

To get the above expression, the approximation $(2M-3)/(M-1) \approx 2$ is used, assuming $M \gg 1$. Thus, unlike the noncoherent integration, the D-PDI technique does not suffer from the SNR wall limitation due to noise uncertainty. This is because the use of cross-terms in the D-PDI technique results in a zero mean under H_0 and mean independent of the noise variance under H_1, which enables the D-PDI method to asymptotically detect very weak signals even in the presence of uncertainty in the noise variance.

Finally, it is straightforward to see that the D-PDI technique is not a robust method in the presence of unknown data-bits. For example, the performance degrades rapidly when the coherent integration duration is half the data-bit period since every other term in (22) spans different data-bits. This performance degradation is illustrated through simulation results in Section VI. In the next section we propose a modified PDI method that is robust to both noise uncertainty as well as unknown data-bits.

V. MODIFIED PDI

We now propose a modified PDI technique that combines the advantages of the NC-PDI and the D-PDI techniques. The motivation for the modified PDI technique comes from the expansion of the ideal coherent integration-based statistic $T = (x[1] + x[2] + \cdots + x[N])(x^*[1] + x^*[2] + \cdots + x^*[N])$, where $x[k]$ represents the coherent integration output after integration for a duration T_{coh}, as before. Here, N is chosen such that the total coherent integration duration NT_{coh} is at most the data-bit duration T_b. The N^2 terms in the expansion can be regrouped and compactly expressed as [10]

$$T = \sum_{l=1}^{N} |x[l]|^2 + 2\text{Re}\left\{\sum_{l=2}^{N} x[l]x^*[l-1]\right\} + \cdots + 2\text{Re}\left\{\sum_{l=n+1}^{N} x[l]x^*[l-n]\right\} + \cdots + 2\text{Re}\{x[N]x^*[1]\}. \quad (37)$$

That is, T is the sum of an NC-PDI term and the k-span D-PDI terms, for $1 \le k \le N-1$.

A. Modified PDI for Data Channel

Consider the following modification of T in (37), in which the NC-PDI term is excluded

$$T_{D1} = \sum_{k=1}^{M} \left\{ \left| \sum_{n=1}^{N} x_k[n] \right|^2 - \sum_{n=1}^{N} |x_k[n]|^2 \right\} \quad (38)$$

where $x_k[n]$ is the coherent integration output in the kth PDI block, with T_{coh} typically a fraction of T_b, and N is the number of coherent integration outputs within a data-bit duration (i.e., $T_{\text{coh}}N \le T_b$).

For example, if the data-bit duration is $T_b = 2T_{\text{coh}}$, each $x_k[n]$ represents a coherent integration output of duration T_{coh}, at the nth ($n \in \{1,2\}$) instant within the span of the kth data-bit block. In this case, the modified PDI test statistic given by (38) is identical to the T_{C1} presented in Section IV and the test statistic employed in [36]

$$T'_{D1} = \sum_{k=1}^{M} x_k[2]x_k^*[1]. \quad (39)$$

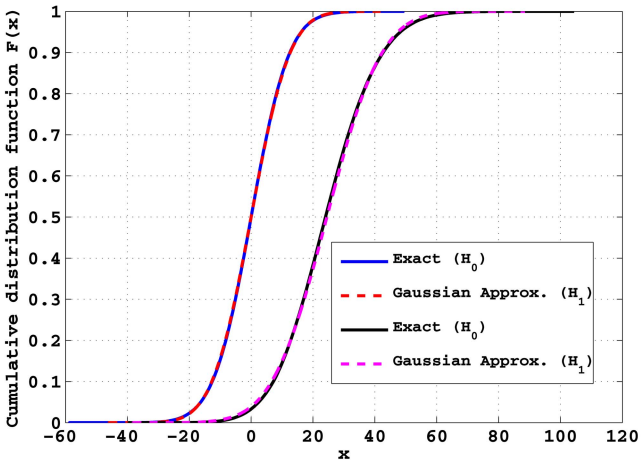

Fig. 4. Empirical cdf to validate Gaussian approximation to cdf of D-PDI test statistic, with $M = 50$, $\rho_{\text{coh}} = -3$ dB.

Note that, by construction, the test statistic T_{D1} is robust to data-bit uncertainty since the test statistic only accumulates the multi-span D-PDI terms computed from samples within a data-bit duration. The robustness to noise uncertainty is also naturally incorporated since the NC-PDI terms are explicitly subtracted out. The robustness of the modified PDI method to uncertainty in the data-bits and noise variance is further corroborated by the simulation results presented in Section VI.

1) *Analytical Characterization*: The kth term in (38) can be expressed in the following quadratic form:

$$T_{D1_k} = X_k^H A X_k \quad (40)$$

where $X_k = [x_k[1], x_k[2], \ldots, x_k[N]]^T$ and A is a symmetric Toeplitz matrix with all elements except the diagonal entries equal to 1, i.e.

$$A = -I_N + \underline{1}\,\underline{1}^T \quad (41)$$

where I_N is the identity matrix of order N and $\underline{1} = [1, 1, \ldots, 1]^T$. The eigenvalues of A are given by $\{N-1, -1, \ldots, -1\}$. Therefore, the test statistic T_{D1_k} can be expressed as a weighted sum of χ^2 random variables, as

$$T_{D1_k} = (N-1)|y_k[1]|^2 - \sum_{n=2}^{N} |y_k[n]|^2 \quad (42)$$

where $y_k[n] = \underline{v}_n^H X_k$ and $\underline{v}_n$ is the eigenvector corresponding to nth eigenvalue of A, which is obtained as in the Appendix, Subsection A. The final test statistic in (38) can be written as

$$T_{D1} = (N-1)\sum_{k=1}^{M} |y_k[1]|^2 - \sum_{k=1}^{M}\sum_{n=2}^{N} |y_k[n]|^2. \quad (43)$$

The P_{fa} expression for the difference of χ^2 random variables each with even degrees of freedom is known

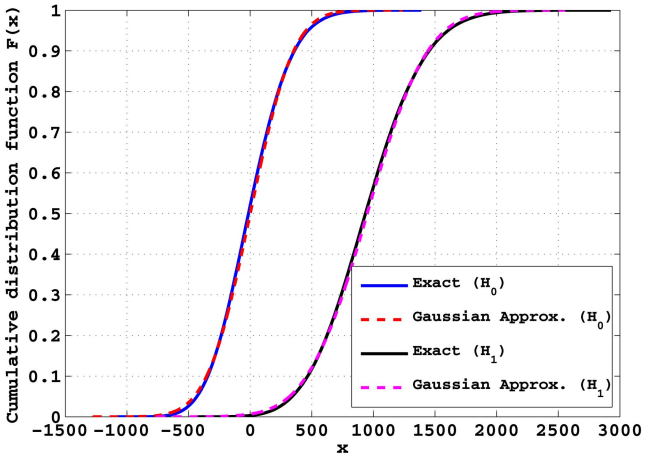

Fig. 5. Empirical cdf and Gaussian-approximated cdf for modified PDI (data channel), $M = 50$, $N = 20$, $\rho_{\text{coh}} = -3$ dB.

[26]. However, as it involves factorials of the order of MN, we resort to the numerical inversion of the characteristic function, as in Section IV. The P_{d} and P_{fa} can be evaluated as in (30). For P_{fa}, the parameters in the integrand, i.e., $\theta_{P_{\text{fa}}}(u)$ and $c_{P_{\text{fa}}}(u)$ are given by

$$\begin{aligned}\theta_{P_{\text{fa}}}(u) &= \sum_{k=1}^{2}[MN_k \tan^{-1}(2\lambda_k N_{\text{coh}}\sigma^2 u)] - \gamma u \\ c_{P_{\text{fa}}}(u) &= \prod_{k=1}^{2}(1+4\lambda_k^2 N_{\text{coh}}^2\sigma^4 u^2)^{MN_k/2}.\end{aligned} \tag{44}$$

Similarly, for evaluating P_{d}

$$\begin{aligned}\theta_{P_{\text{d}}}(u) &= \sum_{k=1}^{2}[MN_k \tan^{-1}(2\lambda_k N_{\text{coh}}\sigma^2 u) + MN_k\mu_{y_k}^2\lambda_k N_{\text{coh}}\sigma^2 u(1+4\lambda_k^2 N_{\text{coh}}^2\sigma^4 u^2)^{-1}] - \gamma u \\ c_{P_{\text{d}}}(u) &= \prod_{k=1}^{2}[(1+4\lambda_k^2 N_{\text{coh}}^2\sigma^4 u^2)^{MN_k/2}]\exp\left(\frac{1}{2}\sum_{k=1}^{2}\frac{MN_k(\mu_{y_k}2\lambda_k N_{\text{coh}}\sigma^2 u)^2}{(1+4\lambda_k^2 N_{\text{coh}}^2\sigma^4 u^2)}\right)\end{aligned} \tag{45}$$

where γ is the detection threshold and N_k is the algebraic multiplicity of the eigenvalue λ_k, which equals 1 and $N-1$ for the eigenvalues $N-1$ and -1, respectively.

2) *Sample Complexity*: As in Section IV, it can be shown that

$$\begin{aligned}E\{T_{D1} \mid H_0\} &= 0 \\ \text{Var}\{T_{D1} \mid H_0\} &= 4MN(N-1)N_{\text{coh}}^2\sigma^4.\end{aligned} \tag{46}$$

Under H_1, it can be shown that the test statistic T_{D1_k} given by (42) can be expressed as the difference of a noncentral and a central chi-square random variable, which results in

$$\begin{aligned}E\{T_{D1_k} \mid H_1\} &= (N-1)(N_{\text{coh}}^2 P\alpha^2 + 2N_{\text{coh}}\sigma^2) - \sum_{k=1}^{N-1}2N_{\text{coh}}\sigma^2 \\ &= (N-1)N_{\text{coh}}^2 P\alpha^2\end{aligned}$$

where $\alpha = \sum_{p=1}^{N} v_{1_p}$, where v_{1_p} is the pth component of $\underline{v}_1$, the eigenvector corresponding to the largest eigenvalue of $(N-1)$. Similarly, it can be shown that

$$\text{Var}\{T_{D1_k} \mid H_1\} = 4(N-1)N_{\text{coh}}\sigma^2(NN_{\text{coh}}\sigma^2 + (N-1)N_{\text{coh}}^2 P\alpha^2).$$

Hence, the mean and variance of the test statistic T_{D1} under H_1 are given by

$$\begin{aligned}E\{T_{D1} \mid H_1\} &= M(N-1)N_{\text{coh}}^2 P\alpha^2 \\ \text{Var}\{T_{D1} \mid H_1\} &= 4M(N-1)N_{\text{coh}}\sigma^2 \\ &\quad \times (NN_{\text{coh}}\sigma^2 + (N-1)N_{\text{coh}}^2 P\alpha^2).\end{aligned} \tag{47}$$

To compute the sample complexity, as before, the expressions for P_{fa} and P_{d} in the presence of noise uncertainty are evaluated by approximating the pdf of T_{D1} with a Gaussian distribution by the moment matching method. From (43), the test statistic T_{D1} can be expressed as the weighted sum of N dependent random variables, each of which is the sum of M i.i.d. random variables with finite variance. Hence, by the CLT, the pdf of the test statistic is well approximated by the Gaussian distribution for large M. The accuracy of the Gaussian approximation is shown in Fig. 5 with $M = 50$, $N = 20$, and a coherent SNR of -3 dB, and it is seen that the agreement between the approximated cdf and the exact cdf is excellent. Thus, the sample complexity can be evaluated as

$$M = \frac{4\left(Q^{-1}(P_{\text{fa},nu})\sqrt{\frac{N}{(N-1)}\beta^2} - Q^{-1}(P_{d,nu})\sqrt{\frac{N}{(N-1)}\frac{1}{\beta^2} + \frac{\rho_{\text{coh}}}{\beta}}\right)^2}{\rho_{\text{coh}}^2} \tag{48}$$

where, with a slight abuse of notation, ρ_{coh} is defined as $N_{\text{coh}}P\alpha^2/\sigma_n^2$. Thus, it is clear that M is bounded in the presence of noise uncertainty and no SNR

limit exists. In summary the proposed modified PDI technique is robust to both uncertainty in the data-bits as well as in the noise variance. Next, we present a version of the modified PDI technique that is applicable to pilot channels.

B. Modified PDI for Pilot Channel

When a pilot channel is available, the coherent integration can span multiple data-bits. Then, using the D-PDI terms with more than one span improves the detection performance in the presence of a small but non-zero frequency offset between the transmitter and the receiver. However, using additional higher span D-PDI terms without compensating for the instantaneous phase shift due to the frequency offset could result in signal degradation [10]. One approach that can be adopted is to treat the unknown frequency offset as a random variable and average over its distribution to obtain the average PDI (A-PDI) [20]. In this work, taking cue from the previous subsection, we modify the A-PDI test statistic by excluding the NC-PDI term in (37) and limiting the span of the D-PDI terms to $L \ll M$. This results in the modified A-PDI test statistic of the form

$$T_{D2} = \sum_{p=1}^{L} \mathrm{Re}\left\{ \sum_{k=p+1}^{M} x[k]x^*[k-p]\mathrm{sinc}(2p\Delta f_{\max} T_{\mathrm{coh}}) \right\} \tag{49}$$

where $\Delta f_{\max}$ is the upper bound on the frequency offset which depends on the frequency resolution of the coarse synchronization stage and L is the number of D-PDI spans included in the test statistic.

1) *Analytical Characterization*: Here, we derive an approximation to the distribution of the test statistic T_{D2}. The test statistic can be expressed in quadratic form as $T_{D2} = X^H A X$, where A is a banded Toeplitz matrix and $X = [x[1], x[2], \ldots, x[M]]^T$. An expression for the eigenvalues of a banded Toeplitz matrix is not known in closed form, except for the tri-diagonal Toeplitz case. However, since $M \gg L$, the asymptotic equivalence of eigenvalues of circulant and banded Toeplitz matrices can be exploited, and a corresponding circulant matrix C can be constructed by a cyclic shift of the row vector deduced from T_{D2}

$$\underline{r}_1 = [0, \mathrm{sinc}(\psi), \mathrm{sinc}(2\psi), \ldots, \mathrm{sinc}(L\psi), 0, \ldots, 0, \mathrm{sinc}(L\psi), \ldots, \mathrm{sinc}(2\psi), \mathrm{sinc}(\psi)]^T \tag{50}$$

where $\psi = 2\Delta f_{\max} T_{\mathrm{coh}}$. The eigenvalues of A converge to the corresponding eigenvalues of C asymptotically [35]. Thus, we use the approximation $T_{D2} \approx X^H C X$ to derive the statistics of T_{D2}. Using the fact that the Fourier basis matrix diagonalizes any circulant matrix [39],

$$T_{D2} \approx (F^H X)^H \Lambda_F (F^H X) \tag{51}$$

where $F \triangleq [\underline{f}_1, \underline{f}_2, \ldots \underline{f}_M]$, and

$$\underline{f}_k = \frac{1}{\sqrt{M}} \left[1, \exp\left\{ -\frac{j2\pi k}{M} \right\}, \exp\left\{ -\frac{j2\pi 2k}{M} \right\}, \ldots, \exp\left\{ -\frac{j2\pi (M-1)k}{M} \right\} \right]^T$$

and $\Lambda_{F_k} = \mathrm{diag}\{\lambda_{F_1}, \lambda_{F_2}, \ldots, \lambda_{F_M}\}$. Thus,

$$T_{D2} \approx \sum_{k=1}^{M} \lambda_{F_k} |y[k]|^2 \tag{52}$$

where $y[k] = \underline{f}_k^H X$. Using (44) and (45), the P_{fa} and P_{d} can now be evaluated by numerically inverting the characteristic function.

2) *Sample Complexity*: The modified A-PDI technique is robust against noise uncertainty as the mean of the test statistic under both the hypotheses is independent of noise variance. The mean and variance under H_1 depend on the instantaneous frequency offset in the data samples since the projection of the data onto the Fourier basis varies with the frequency offset. The mean and variance of the test statistic with the modified A-PDI technique is presented in a generalized form in terms of the eigen-values and eigen-vectors of the circulant matrix C defined above. Computing the mean of T_{D2} under either hypothesis, it can be shown that

$$\begin{aligned} E\{T_{D2} \mid H_0\} &= 2N_{\mathrm{coh}}\sigma^2 \sum_{k=1}^{M} \lambda_{F_k} = \mathrm{Tr}\{C\} = 0 \\ E\{T_{D2} \mid H_1\} &= \sum_{k=1}^{M} \lambda_{F_k} |\underline{f}_k^H \underline{\mu}_k|^2 \end{aligned} \tag{53}$$

where $\mu_k = E\{X \mid H_1\}$. Similarly, using the fact that the test statistic is a weighted sum of central χ^2 random variables under H_0 and is a weighted sum of noncentral χ^2 random variables under H_1, the expression for the variance of the test statistic under either hypothesis is given by

$$\begin{aligned} \mathrm{Var}\{T_{D2} \mid H_0\} &= 4N_{\mathrm{coh}}^2\sigma^4 \sum_{k=1}^{M} \lambda_{F_k}^2 \\ \mathrm{Var}\{T_{D2} \mid H_1\} &= 4N_{\mathrm{coh}}\sigma^2 \left(\sum_{k=1}^{M} \lambda_{F_k}^2 N_{\mathrm{coh}}\sigma^2 + \lambda_{F_k}^2 |\underline{f}_k^H \underline{\mu}_k|^2 \right). \end{aligned} \tag{54}$$

As in the previous subsection, the sample complexity can now be computed using Gaussian approximations. The test statistic T_{D2} in (49) can be viewed as the weighted sum of L dependent random variables, each

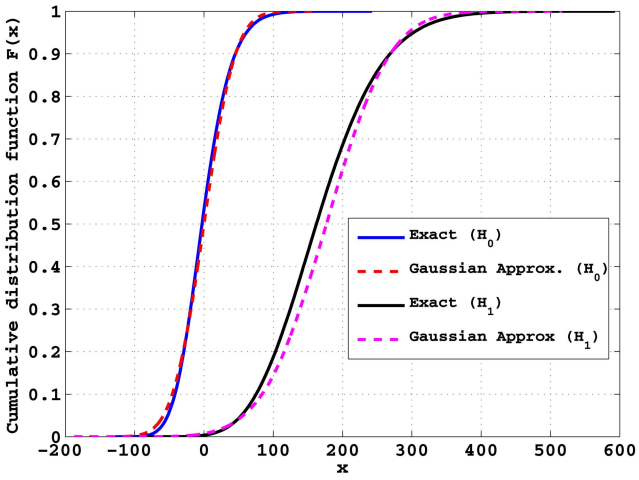

Fig. 6. Empirical cdf to validate Gaussian approximation of cdf of modified PDI (pilot channel), $M = 50$, $\rho_{\text{coh}} = -3$ dB, 4-span D-PDI.

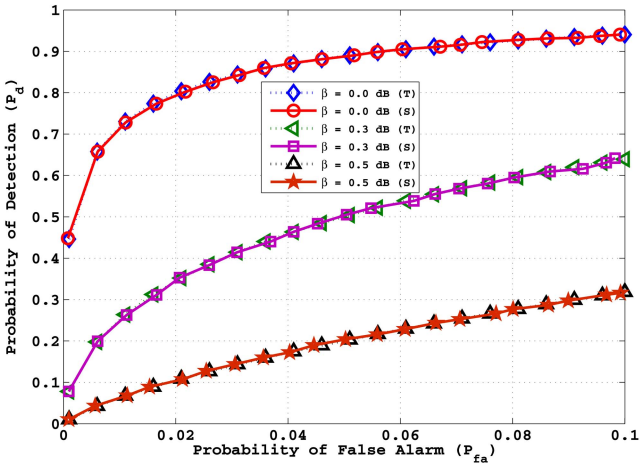

Fig. 7. ROC of NC-PDI (quadratic form) with and without noise uncertainty, $M = 100$, $\rho_{\text{coh}} = -2$ dB.

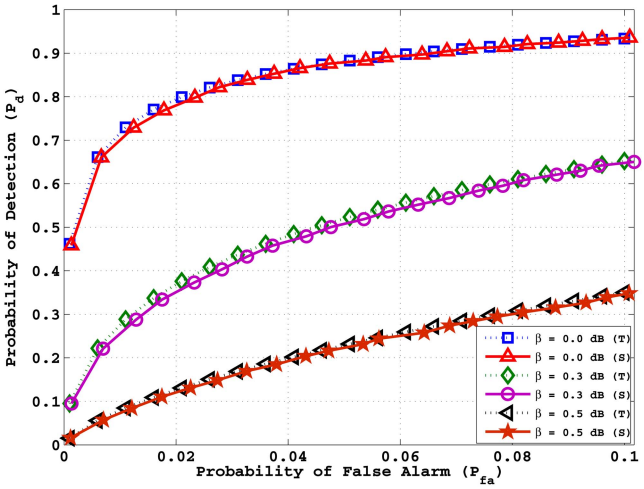

Fig. 8. ROC of NC-PDI (nonquadratic form) with and without noise uncertainty, $M = 100$, $\rho_{\text{coh}} = -2$ dB.

of which is the sum of at least $M - L$ i.i.d. random variables with finite variance. Hence, by the CLT, the pdf of the test statistic is well approximated by the Gaussian distribution for large M. Figure 6 compares the empirical cdf obtained via computer simulations with the Gaussian approximation for the case of a 4-span D-PDI with $M = 50$ and a coherent SNR of -3 dB. We see that the approximation error is small, although not as good as in the previous sections. Yet, it is shown in the next section that the effect of the error in the approximation on the computed P_{fa} and P_{d} values is negligible. The sample complexity with and without noise uncertainty can also be obtained using the above expressions.

VI. SIMULATION RESULTS

This section presents Monte Carlo simulation results to verify the theoretical expressions derived above and to illustrate the performance improvement offered by the proposed modified PDI technique. The detection performance of the different PDI techniques is quantified through the receiver operating characteristic (ROC) curves. The simulation setup is as follows. The SNR at the output of the coherent integration stage is taken as -2 dB. The sample complexity of the NC-PDI technique is set as $M = 100$. The coherent processing assumes accurate alignment to data-bit boundary as this permits the maximum possible coherent processing for a given data rate. Since the focus here is on data-bit and noise uncertainty, the effects of frequency and time offsets are ignored in the simulations, unless stated otherwise.

In Fig. 7, the plot of the ROC for the quadratic NC-PDI technique with noise uncertainty of 0 dB (i.e., no noise uncertainty), 0.3 dB, and 0.5 dB is shown. The theoretical plots of the ROC are evaluated from (6), and the close match between the theoretical and experimental curves is clear. Also, the detection performance degrades as β increases, and if the noise uncertainty is increased further, the ROC curve need not remain concave.

In Fig. 8, the ROC plots for the nonquadratic NC-PDI discussed in Section III are shown. The expressions in (19) and (20) are used to generate the theoretical curves marked (T); and the simulation-based curves are marked (S). The performance degradation of the quadratic and nonquadratic PDI due to noise uncertainty are similar. Thus, in general, the NC-PDI techniques are not robust to noise uncertainty.

In Fig. 9, the ROC curves with and without noise uncertainty are plotted, for the D-PDI technique. Here, a coherent processing duration of half the data-bit duration is employed, with a signal with coherent SNR of -2 dB and a sample complexity of $M = 50$. In contrast with NC-PDI, the D-PDI offers a 1.5 dB improvement for the same value of M over NC-PDI [36], because of the so-called squaring loss in the latter [31, 12], NC-PDI [36], and hence, the value of

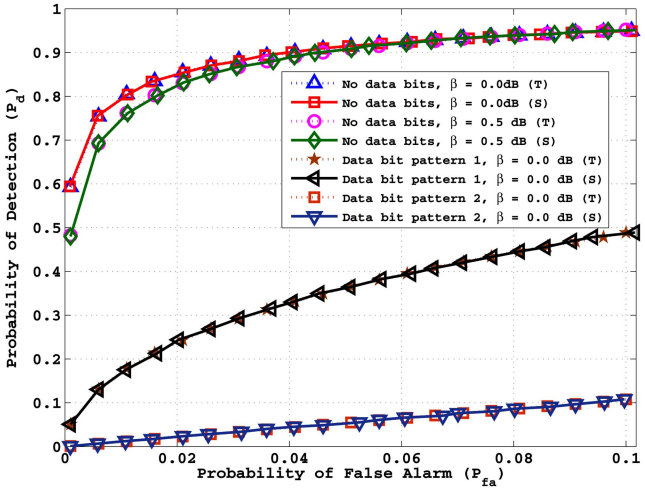

Fig. 9. ROC of D-PDI method with and without noise uncertainty, $T_{\text{coh}} = (T_b/2)$ms, $M = 50$, $\rho_{\text{coh}} = -2$ dB.

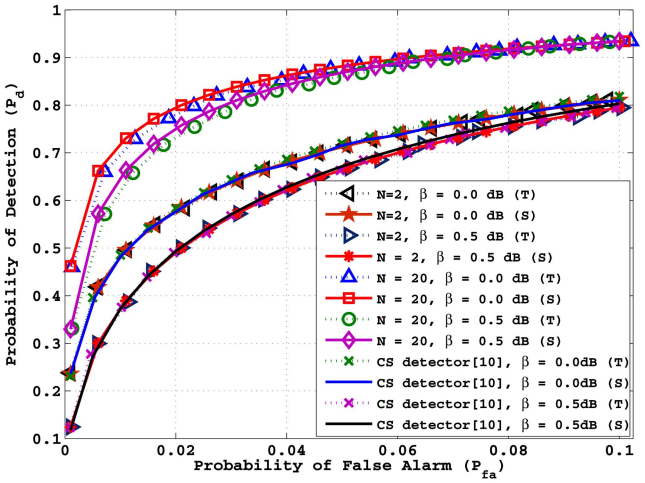

Fig. 10. ROC of modified PDI for data channel with and without noise uncertainty, $M = 100$, $\rho_{\text{coh}} = -2$ dB.

$M = 50$ ensures that the comparison with the NC-PDI method is fair. The expressions in (27) and (30) are used to plot the theoretical curves. It is clear from the plot that there is only a slight degradation in performance due to noise uncertainty, caused because the threshold is set based on the largest possible noise variance. The curves marked "no data-bits" refer to the case where all data-bits are $+1$. The curves marked "data-bit pattern 1" and "data-bit pattern 2" represent the performance when the data is i.i.d. Bernoulli distributed and when the data sequence is alternate $+1$ and -1, respectively. In the presence of data-bits, with a coherent integration duration of half the data-bit duration (for example, 10 ms in the case of GNSS signal detection), the odd terms of the test statistic straddle adjacent data-bits. Due to this, there is a severe degradation in the performance of the D-PDI technique.

Figure 10 shows the performance of the modified PDI technique for a data channel proposed in this paper, along with the theoretical expressions obtained in (44) and (45). From the figure, it can be seen that in the presence of noise uncertainty the performance degradation is small, similar to the D-PDI technique. Also, it is interesting to note that the test statistic in (38) with $N = 20$, $T_{\text{coh}} = T_b/20$ offers better performance than $N = 2$ and $T_{\text{coh}} = T_b/2$ (recall that $N_{\text{coh}} = f_s T_{\text{coh}}$). This is because the signal induced bias in the noise variance term causes part of the signal in the test statistic to get canceled out, leading to poor performance as the coherent integration duration increases. Thus, the proposed scheme is robust against the artefacts introduced due to uncertainty in both noise variance and data-bits. Finally, the performance of the proposed modified PDI technique is compared with that of the cyclostationarity-based detector proposed in [18] (curves marked "CS detector"). To keep the comparison fair, the cyclostationarity-based detector is simulated with $M = 200$ and an SNR of -5 dB. This keeps the dwell time (equal to $(100T_b)$) the same for both detectors and also accounts for the fact that the maximum coherent integration duration for the cyclostationarity-based detector is $T_b/2$. The performance of the cyclostationarity-based detector closely matches that of the modified PDI with $N = 2$ and $T_{\text{coh}} = T_b/2$. This is as expected since the modified PDI detector reduces to the cyclostationary detector when the test statistic is the sum (rather than an arbitrary convex combination) of two cyclic frequency components. However, the proposed modified PDI technique with $N = 20$ clearly outperforms the cyclostationarity-based detector.

In Fig. 11, the performance of the modified PDI technique for a pilot channel proposed in this paper is shown, with the theoretical curves plotted using the inversion of the characteristic function, as explained in Section V-B. In the presence of a non-zero frequency offset, the number of spans used in the test statistic needs to be limited. In the simulation, two and four spans are considered, and these correspond to a maximum frequency offset of $\Delta f_{\max} T_{\text{coh}} = 0.2$ and $\Delta f_{\max} T_{\text{coh}} = 0.1$, respectively. The sample complexity is set as $M = 50$. From the ROC plots, it is observed that there is a significant improvement in the 4-span D-PDI compared with the 2-span and 1-span D-PDI cases. However, the frequency search resolution in the coarse synchronization stage limits the number of additional spans that can be used in computing the test statistic. Also, note that the circulant approximation for the banded Toeplitz structure closely matches the performance of the modified PDI test statistic.

In Fig. 12, the sample complexity for the NC-PDI technique is shown as a function of the coherent SNR ρ_{coh}. Two different noise uncertainty values are used: $\beta = 0.3$ dB for the quadratic case and

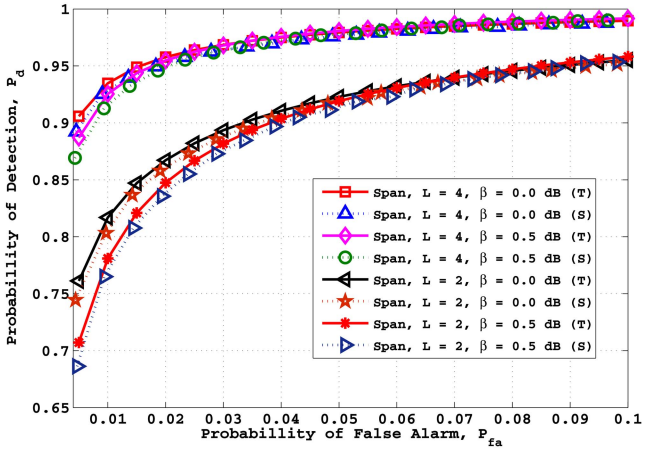

Fig. 11. ROC of modified PDI for pilot channel with and without noise uncertainty, $M = 50$, $\rho_{\text{coh}} = -2$ dB.

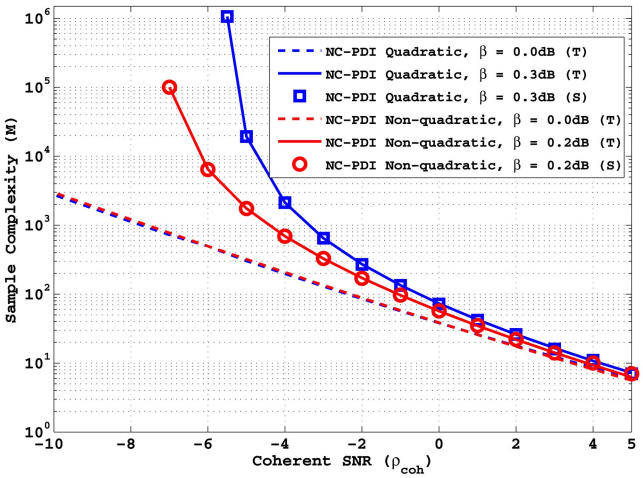

Fig. 12. Sample complexity versus coherent SNR (NC-PDI quadratic and NC-PDI nonquadratic): $P_{\text{fa}} = 0.1$ and $P_{\text{d}} = 0.9$.

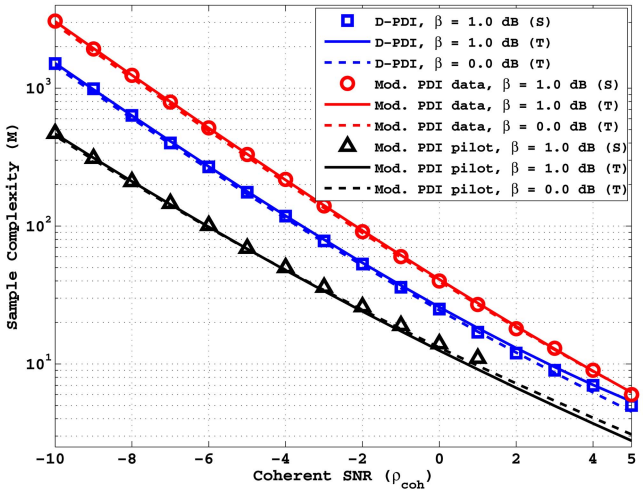

Fig. 13. Sample complexity versus coherent SNR (D-PDI, modified PDI data, modified PDI pilot): $P_{\text{fa}} = 0.1$ and $P_{\text{d}} = 0.9$.

$\beta = 0.2$ dB for the nonquadratic case. In the presence of noise uncertainty, the sample complexity becomes unbounded as the coherent SNR decreases. Figure 13 shows a similar plot for the D-PDI and modified PDI techniques. The performance degradation is small even in the presence of noise uncertainty of magnitude $\beta = 1$ dB. The parameter N in the modified PDI technique for data is set to 20, and in the case of the modified PDI for the pilot channel, the number of spans L is set to 4 and $\Delta f T_{\text{coh}} = 0$. The simulation results closely match the theoretical values.

Finally, we consider a case study of a typical GNSS receiver. The noise floor is assumed to be at -111 dBm [28]. If the coherent integration duration $T_{\text{coh}} = 10$ ms and the noise uncertainty is 0.3 dB, reliable signal detection is not possible, and the sample complexity $M \to \infty$, when the SNR at the output of the coherent integration stage drops below $\rho_{\text{coh}} = -5.6$ dB. This corresponds to an SNR of $\text{SNR}_L = -48.7$ dB at the input to the coherent integration stage, i.e., to an input signal strength of -159.7 dBm.[1] Current state-of-the-art GNSS receivers are capable of detecting signals with SNR as low as -157 dBm in an indoor environment [37]. Thus, the lowest SNR for reliable detection with current technology is only 2.7 dB away from the SNR wall due to a 0.3 dB noise uncertainty.

VII. CONCLUSIONS

This paper studied the performance of two popular suboptimal PDI techniques, namely, the NC-PDI and the D-PDI, under uncertainties in the frequency, timing, noise variance, and the data-bit sequence. It was demonstrated that the NC-PDI was robust to the data-bit uncertainty, but its performance severely degrades under noise uncertainty. In particular, it was shown that a fundamental lower limit on the SNR for reliable detection exists under noise uncertainty in the NC-PDI technique, in both the quadratic and nonquadratic forms. It was also shown that the D-PDI technique is inherently robust to noise uncertainty, but its performance is nonrobust in the presence of data-bit polarity changes. A robust modified PDI technique that combines the advantages of both the D-PDI and NC-PDI techniques was proposed. A detailed analytical characterization of the probabilities of false alarm and detection, as well as of the sample complexity required to achieve a given performance level, was derived for all the detectors considered. Monte Carlo simulations illustrated the accuracy of the theoretical expressions and the performance improvement offered by the proposed technique in the face of uncertainty in the noise variance and data-bit polarities. Future work could include quantifying the magnitude of noise uncertainty in GNSS systems,

[1] The gain from the coherent integration duration of 10 ms is about 43.1 dB [28].

demonstrating its effect, and validating the robustness of the proposed detectors in practical receivers.

APPENDIX

A. 1-Span D-PDI as a Weighted Sum of χ^2 Random Variables

Here, it is shown that the 1-span D-PDI test statistic can be expressed as a weighted sum of independent χ^2 random variables. The test statistic $T_C = \mathrm{Re}\{\sum_{k=2}^{M} x[k]x^*[k-1]\}$ can be expressed in the quadratic form as $X^H AX$, where $X = [x[1],x[2]\ldots x[M]]^T$ and A is a tri-diagonal Toeplitz matrix [38]. From [39], its eigenvalues are given by

$$\lambda_k = \cos\left(\frac{\pi k}{M+1}\right). \tag{55}$$

The corresponding eigenvectors form an orthonormal basis as A is a symmetric matrix. The kth eigenvector is represented as

$$v_k = \left[\sin\left(\frac{k\pi}{M+1}\right) \quad \sin\left(\frac{2k\pi}{M+1}\right) \right.$$
$$\left. \sin\left(\frac{3k\pi}{M+1}\right)\cdots\sin\left(\frac{Mk\pi}{M+1}\right)\right]^H. \tag{56}$$

Using this, the test statistic T_C can be expressed as

$$T_C = (V^H X)^H \Lambda V^H X$$

where $V \triangleq [\underline{v}_1,\underline{v}_2,\ldots,\underline{v}_M]$ is the eigenvector matrix, Λ is a diagonal matrix with the eigenvalues of A as its diagonal elements, and $\Lambda = \mathrm{diag}(\lambda_1,\lambda_2,\ldots,\lambda_M)$. The test statistic T_C can now be written as

$$T_C = \sum_{k=1}^{M} \lambda_k |y[k]|^2$$

where $y[k] = \underline{v}_k^H X$ is an orthogonal linear transformation of X. It is now straightforward to show that

$$y[k] \sim \begin{cases} CN(0,N_{\mathrm{coh}}\sigma^2), & \text{under } H_0 \\ CN(\underline{v}_k^H \underline{\mu}_X, N_{\mathrm{coh}}\sigma^2), & \text{under } H_1. \end{cases}$$

Thus, $|y[k]|^2$ is a χ^2 random variable with two degrees of freedom. So, the 1-span D-PDI test statistic can be expressed as a linear combination of independent χ^2 random variables. Note that the above test statistic is an indefinite quadratic form, as both negative and positive eigenvalues are present. The M eigenvalues can be grouped into $M/2$ pairs of antisymmetric eigenvalues. This gives an alternative representation of the 1-span D-PDI test statistic as the weighted sum of the difference between two χ^2 random variables

$$T_C = \sum_{k=1}^{M/2} \lambda_k (|y_p[k]|^2 - |y_n[k]|^2)$$

where $y_p[k]$ and $y_n[k]$ represent the components of $y[k]$ corresponding to the positive and negative eigenvalues, respectively. The above analysis holds for both even and odd values of M.

B. Cross-Covariance of T_{C1} and T_{C2}

Here, the cross-covariance of the two random variables T_{C1} and T_{C2} under both hypotheses is evaluated. Substituting for T_{C1} and T_{C2} from (33), a typical term in the resulting expression is given by

$$E\{(x_I[2m]x_I[2m-1] + x_Q[2m]x_Q[2m-1])$$
$$\times (x_I[2l+1]x_I[2l] + x_Q[2l+1]x_Q[2l])\}. \tag{57}$$

The $x_I[k]$s and $x_Q[k]$s are i.i.d. Gaussian random variables. The term inside the expectation above is of one of the following three mutually exclusive forms: $m = l+1$, $m = l$, or $m \neq l, l+1$. In all three cases, it is straightforward to show that the expectation under H_0 is zero.

To evaluate the cross-covariance under hypothesis H_1, we again recognize that the term in (57) is of one of the following three forms.

Case 1 $m = l+1$: It can be shown that the four terms in the expansion of (57) evaluate to

$$\begin{aligned} E\{x_I[2l+2]\}E\{x_I^2[2l+1]\}E\{x_I[2l]\} &= N_{\mathrm{coh}}^4 P^2 \cos^4\theta + N_{\mathrm{coh}}^3 P\sigma^2\cos^2\theta \\ E\{x_I[2l+2]\}E\{x_I[2l+1]\}E\{x_Q[2l+1]\}E\{x_Q[2l]\} &= N_{\mathrm{coh}}^4 P^2 \cos^2\theta\sin^2\theta \\ E\{x_Q[2l+2]\}E\{x_Q[2l+1]\}E\{x_I[2l+1]\}E\{x_I[2l]\} &= N_{\mathrm{coh}}^4 P^2 \cos^2\theta\sin^2\theta \\ E\{x_Q[2l+2]\}E\{x_Q^2[2l+1]\}E\{x_I[2l]\} &= N_{\mathrm{coh}}^4 P^2 \sin^4\theta + N_{\mathrm{coh}}^3 P\sigma^2\sin^2\theta \end{aligned} \tag{58}$$

where θ is the unknown phase offset, as in (2). Putting the above four terms together, when $m = l+1$, a typical term as in (57) simplifies to $N_{\mathrm{coh}}^4 P^2 + N_{\mathrm{coh}}^3 P\sigma^2$.

Case 2 $m = l$: Similarly, it can be shown that a typical term in (57) again evaluates to $N_{\mathrm{coh}}^4 P^2 + N_{\mathrm{coh}}^3 P\sigma^2$.

Case 3 $m \neq l, l+1$*:* In this case, the expression results in terms of the following form, with $p \neq q$:

$$\begin{aligned}
E\{x_I[2l+p]\}E\{x_I[2l+q]\}E\{x_I[2l+1]\}E\{x_I[2l]\} &= N_{\text{coh}}^4 P^2 \cos^4\theta \\
E\{x_I[2l+p]\}E\{x_I[2l+q]\}E\{x_Q[2l+1]\}E\{x_Q[2l]\} &= N_{\text{coh}}^4 P^2 \cos^2\theta \sin^2(\theta) \\
E\{x_Q[2l+p]\}E\{x_Q[2l+q]\}E\{x_I[2l+1]\}E\{x_I[2l]\} &= N_{\text{coh}}^4 P^2 \cos^2\theta \sin^2(\theta) \\
E\{x_Q[2l+p]\}E\{x_Q[2l+q]\}E\{x_Q[2l+1]\}E\{x_Q[2l]\} &= N_{\text{coh}}^4 P^2 \sin^4\theta.
\end{aligned} \tag{59}$$

The sum of the above terms evaluates to $N_{\text{coh}}^4 P^2$.

Putting the above cases together, there are $M/2$ terms such that $m = l+1$, $M/2-2$ terms such that $m = l$, and the remaining $(M/2-1)(M/2-2)$ terms correspond to $m \neq l, l+1$. Therefore, we have

$$E\{T_{C1}T_{C2}\} = \frac{M}{2}\left(\frac{M}{2}-1\right)N_{\text{coh}}^4 P^2 + (M-2)N_{\text{coh}}^3 P\sigma^2. \tag{60}$$

Since $E\{T_{C1}\} = (M/2)N_{\text{coh}}^2 P$ and $E\{T_{C2}\} = ((M/2)-1)\cdot N_{\text{coh}}^2 P$, the covariance $\text{Cov}(T_{C1}, T_{C2})$ under H_1 is

$$\begin{aligned}
\text{Cov}(T_{C1}, T_{C2}) &= E\{T_{C1}T_{C2}\} - E\{T_{C1}\}E\{T_{C2}\} \\
&= (M-2)N_{\text{coh}}^3 P\sigma^2.
\end{aligned} \tag{61}$$

Thus, the variance of the 1-span D-PDI test statistic under H_1 is given by

$$\text{Var}\{T_C \mid H_1\} = 2(M-1)N_{\text{coh}}^2\sigma^4 + 2(2M-3)N_{\text{coh}}^3 P\sigma^2. \tag{62}$$

REFERENCES

[1] Viterbi, A. J.
CDMA: Principles of Spread Spectrum Communication (Addison-Wesley Wireless Communications Series). Upper Saddle River, NJ: Prentice-Hall, 1995.

[2] Amar, A., Leus, G., and Friedlander, B.
Emitter localization given time delay and frequency shift measurements.
IEEE Transactions on Aerospace and Electronic Systems, **48**, 2 (Apr. 2012), 1826–1837.

[3] Borio, D., Camoriano, L., and Lo Presti, L.
Impact of GPS acquisition strategy on decision probabilities.
IEEE Transactions on Aerospace and Electronic Systems, **44**, 3 (July 2008), 996–1011.

[4] Corazza, G. E.
On the MAX/TC criterion for code acquisition and its application to DS-SSMA systems.
IEEE Transactions on Communications, **44**, 9 (Sept. 1996), 1173–1182.

[5] Driscoll, C. O.
Performance analysis of the parallel acquisition of weak GPS signals.
Ph.D. dissertation, National University of Ireland, Dublin, Ireland, Jan. 2007.

[6] Huang, K. S. and Weng, C. T.
An innovative self-generated assistance technology for a high sensitivity GPS mobile phone.
Proceedings of International Technical Meeting of the Satellite Division of The Institute of Navigation (ION GNSS), Portland, OR, Sept. 2010, pp. 2981–2985.

[7] Weng, C. T., et al.
An efficient method of self-generated assistance data for fast-fix applications.
Proceedings of International Technical Meeting of the Satellite Division of The Institute of Navigation (ION GNSS), Portland, OR, Sept. 2011, pp. 3967–3974.

[8] Broumandan, A. and Lachapelle, G.
Coherent integration time limit of a mobile receiver for indoor GNSS applications.
GPS Solutions, **16**, 2 (Apr. 2012), 157–167.

[9] Watson, J. R., Lachapelle, G., and Klukas, R.
Testing oscillator stability as a limiting factor in extreme high-sensitivity GPS applications.
Proceedings of the European Navigation Conference (ENC), Manchester, UK, May 2006.

[10] Corazza, G. E. and Pedone, R.
Generalized and average likelihood ratio testing for post detection integration.
IEEE Transactions on Communications, **55**, 11 (Nov. 2007), 2159–2171.

[11] Borio, D. and Akos, D.
Noncoherent integrations for GNSS detection: Analysis and comparisons.
IEEE Transactions on Aerospace and Electronic Systems, **45**, 1 (Jan. 2009), 360–375.

[12] Zarrabizadeh, M. H. and Sousa, E. S.
A differentially coherent PN code acquisition receiver for CDMA systems.
IEEE Transactions on Communications, **45**, 11 (Nov. 1997), 1456–1465.

[13] Tandra, R. and Sahai, A.
SNR walls for signal detection.
IEEE Journal of Selected Topics in Signal Processing, **2**, 1 (Feb. 2008), 4–17.

[14] Chandrasekhar, J. and Murthy, C. R.
GNSS signal detection under noise uncertainty.
Proceedings of the 2010 IEEE International Conference on Communications (ICC), Cape Town, South Africa, May 2010, pp. 1–5.

[15] Boumard, S.
Novel noise variance and SNR estimation algorithm for wireless MIMO OFDM systems.
Proceedings of the IEEE Global Telecommunications Conference (GLOBECOM '03), vol. 3, San Francisco, CA, Dec. 2003, pp. 1330–1334.

[16] Fei, J., Guangliang, R., and Zhe, Z.
A new noise variance and post detection SNR estimation method for MIMO OFDM systems.
Proceedings of the 11th IEEE International Conference Communications Technology (ICCT 2008), Hangzhou, China, Dec. 2008, pp. 179–182.

[17] Das, A. and Rao, B. D.
SNR and noise variance estimation for MIMO systems.
IEEE Transactions on Signal Processing, **60**, 8 (Aug. 2012), 3929–3941.

[18] Chandrasekhar, J. and Murthy, C. R.
Robust GNSS signal detection in the presence of navigation data bits.
Proceedings of the 2011 IEEE International Conference on Acoustics, Speech and Signal Processing (ICASSP), Prague, Czech Republic, May 2011, pp. 4344–4347.

[19] Pulikkoonattu, R. and Antweiler, M.
Analysis of differential non coherent detection scheme for CDMA pseudo random (PN) code acquisition.
Proceedings of the 2004 IEEE Eighth International Symposium on Spread Spectrum Techniques and Applications, Sydney, Australia, Aug. 30–Sept. 2, 2004, pp. 212–217.

[20] Villanti, M., Salmi, P., and Corazza, G. E.
Differential post detection integration techniques for robust code acquisition.
IEEE Transactions on Communications, **55**, 11 (Nov. 2007), 2172–2184.

[21] Van Dierendonck, A. J.
GPS receivers.
In B. W. Parkinson (Ed.), *Global Positioning System: Theory and Applications* (Progress in Astronautics and Aeronautics), vol. 163, Reston, VA: AIAA, 1996, ch. 8.

[22] Chawla, K. K. and Sarwate, D. V.
Parallel acquisition of PN sequences in DS/SS systems.
IEEE Transactions on Communications, **42** (May 1994), 2155–2164.

[23] Weill, L. R.
Theoretical and practical sensitivity limits for assisted GNSS receivers using legacy and future GNSS signals.
Proceedings of the 19th International Technical Meeting of the Satellite Division of The Institute of Navigation (ION GNSS 2006), Fort Worth, TX, Sept. 2006, pp. 2930–2943.

[24] McBurney, P. W.
Design considerations for positioning systems in urban environments.
Proceedings of the European Signal Processing Conference (EUSIPCO), Tampere, Finland, Sept. 2000.

[25] Psiaki, M. L.
Block acquisition of weak GPS signals in a software receiver.
Proceedings of the 14th International Technical Meeting of the Satellite Division of The Institute of Navigation (ION GPS 2001), Salt Lake City, UT, Sept. 2001, pp. 2838–2850.

[26] Simon, M. K.
Probability Distributions Involving Gaussian Random Variables.
Boston, MA: Kluwer, 2002.

[27] Mills, R. F. and Prescott, G. E.
A comparison of various radiometer detection models.
IEEE Transactions on Aerospace and Electronic Systems, **32**, 1 (Jan. 1996), 467–473.

[28] Diggelen, F. V.
AGPS: Assisted GPS, GNSS, and SBAS.
Norwood, MA: Artech House, 2009.

[29] van Diggelen, F.
Indoor GPS theory & implementation.
Proceedings of the 2002 IEEE Position, Location, and Navigation Symposium (PLANS), Palm Springs, FL, Aug. 2002, pp. 240–247.

[30] Shanmugam, S., et al.
Differential signal processing schemes for enhanced GPS acquisition.
Proceedings of the 18th International Technical Meeting of the Satellite Division of The Institute of Navigation (ION GNSS 2005), Long Beach, CA, Sept. 2005, pp. 212–222.

[31] Lowe, S.
Voltage signal-to-noise ratio (SNR) nonlinearity resulting from incoherent summations.
Jet Propulsion Lab (JPL-NASA), Pasadena, CA, Technical Report, 1999.

[32] Kim, P., et al.
Robust frame synchronization for the DVB-S2 system with large frequency offsets.
International Journal of Satellite Communications and Networking, **27**, 1 (Jan. 2009), 35–52.

[33] Kay, S. M.
Fundamentals of Statistical Signal Processing: Detection Theory, vol. 2.
Upper Saddle River, NJ: Prentice-Hall, 1998.

[34] Imhof, J. P.
Computing the distribution of quadratic forms in normal variables.
Biometrika, **48**, 2 (1961), 419–426.

[35] Moon, T. K. and Stirling, W. C.
Mathematical Methods and Algorithms for Signal Processing.
Delhi, India: Pearson, 2005.

[36] Borio, D., et al.
The output SNR and its role in quantifying GNSS signal acquisition performance.
Proceedings of the 2008 European Navigation Conference (ENC 2008), Toulouse, France, Apr. 2008.

[37] Pany, T., et al.
On the state-of-the-art of real-time GNSS signal acquisition—A comparison of time and frequency domain methods.
Proceedings of the 2010 International Conference on Indoor Positioning and Indoor Navigation (IPIN), Zurich, Switzerland, Sept. 2010, pp. 1–8.

[38] Jeong, Y. K., Shin, O. S., and Lee, K. B.
Fast slot synchronization for inter-cell asynchronous DS/CDMA systems.
IEEE Transactions on Wireless Communications, **45**, 11 (Apr. 2002), 1456–1465.

[39] Meyer, C.
Matrix Analysis and Applied Linear Algebra.
Philadelphia, PA: SIAM, 2000.

Chandrasekhar Jayaram received his B.E. degree in electronics and communication engineering from Bangalore University, Bangalore, India in 2004 and his M.Sc (Engg.) degree from the Indian Institute of Science, Bangalore, India in 2011.

He is currently working as a senior engineer at Accord Software and Systems Pvt. Ltd., Bangalore, India. His research interests include detection theory and signal processing for navigation.

Chandra R. Murthy (S'03—M'06—SM'11) received his B.Tech. degree in electrical engineering from the Indian Institute of Technology, Madras, India in 1998, and his M.S. and Ph.D. degrees in electrical and computer engineering from Purdue University, West Lafayette, IN, and the University of California, San Diego, CA, in 2000 and 2006, respectively.

From 2000 to 2002 he worked as an engineer for Qualcomm Inc., San Jose, CA, where he worked on WCDMA baseband transceiver design and 802.11b baseband receivers. From August 2006 to August 2007, he worked as a staff engineer at Beceem Communications Inc., Bangalore, India, on advanced receiver architectures for the 802.16e Mobile WiMAX standard. In September 2007 he joined as assistant professor with the Department of Electrical Communication Engineering at the Indian Institute of Science, Bangalore, India, where he is currently working. His research interests are in the areas of cognitive radio, energy harvesting wireless sensors, and MIMO systems with channel-state feedback. He is currently serving as an associate editor for *IEEE Signal Processing Letters*.